Journal of Hazardous Materials 380 (2019) 120864

Contents lists available at ScienceDirect

Journal of Hazardous Materials

journal homepage: www.elsevier.com/locate/jhazmat

Hierarchical porous carbon material restricted Au catalyst for highly catalytic reduction of nitroaromatics

Lei Qin[a,b,1], Huan Yi[a,b,1], Guangming Zeng[a,b,*], Cui Lai[a,b,*], Danlian Huang[a,b], Piao Xu[a,b], Yukui Fu[a,b], Jiangfan He[a,b], Bisheng Li[a,b], Chen Zhang[a,b], Min Cheng[a,b], Han Wang[a,b], Xigui Liu[a,b]

[a] College of Environmental Science and Engineering, Hunan University, Changsha, 410082, PR China
[b] Key Laboratory of Environmental Biology and Pollution Control, Hunan University, Ministry of Education, PR China

GRAPHICAL ABSTRACT

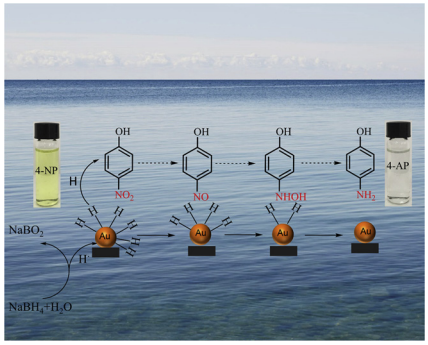

ARTICLE INFO

Keywords:
Au catalysts
Carbon black
Hierarchical porous carbon
Nitroaromatics
Reduction

ABSTRACT

In this study, four kinds of porous carbon materials were used as supports to anchor gold nanoparticles (AuNPs) for catalytic reduction of nitroaromatics and 4-nitrophenol (4-NP) was employed as a model material. Results identified that carbon black (CB) restricted-Au catalyst (Au/CB) provided large specific surface area, small AuNPs size, and low cost, which showed highly catalytic activity for 4-NP reduction. Besides, with the increase of Au loadings, the catalytic activity of Au/CB was enhanced and the 1.2 wt% of Au loading exhibited the best catalytic activity with the high rate of 0.8302 min^{-1} and the turnover frequency of 492.50 h^{-1}. Universality and real water application demonstrated that the as-prepared Au/CB catalyst was promising candidate for other phenols and azo dyes reduction and had great potential for practical application. Furthermore, after ten cycles, Au/CB still retained satisfying stability and activity. These results suggested that the larger specific surface area and smaller particle size attributing to the porosity of CB were conducive to improving the catalytic activity of Au catalysts. This design shows high potential of hierarchical porous carbon materials for highly catalytic reaction in many fields, especially the water purification.

* Corresponding authors at: College of Environmental Science and Engineering, Hunan University, Changsha, Hunan, 410082, PR China
E-mail addresses: zgming@hnu.edu.cn (G. Zeng), laicui@hnu.edu.cn (C. Lai).
[1] These authors contribute equally to this article.

https://doi.org/10.1016/j.jhazmat.2019.120864
Received 10 April 2019; Received in revised form 3 July 2019; Accepted 3 July 2019
Available online 04 July 2019
0304-3894/

1. Introduction

Nowadays, human is facing the severe threat of environmental pollution since the rapid development of industrialization, especially the water pollution (Li et al., 2018; Cheng et al., 2018; Xu et al., 2012; Yi et al., 2019; Wang et al., 2018; Li et al., 2019). The pollutants enter into plants and animals through water circulation and finally accumulate in human body, which can induce serious body damage (Lai et al., 2016; Gong et al., 2017; Xue et al., 2018; Luo et al., 2019; Yang et al., 2018). Nitroaromatics, mainly generated from industry and agriculture, are known as the hazardous and toxic pollutant (Abazari et al., 2019). In particular, 4-nitrophenol (4-NP) as a kind of typical nitroaromatic is considered as one of the most common pollutant in environmental water and industrial wastewater (Song et al., 2019; Guo et al., 2018). It is highly toxic and can result in liver, kidney, central nervous system, and blood system damage (Abdullah et al., 2019; Hu et al., 2018). However, these pollutants are difficult to remove because of the high structural stability. Thus, it is important to develop efficient method to remove them from water.

As one kind of stable and non-toxic nanoparticles, gold nanoparticles (AuNPs) have been widely used in many fields especially environmental protection due to its excellent properties (Ciriminna et al., 2016; Liu et al., 2018; Qin et al., 2017; Scurrell, 2017; Ai et al., 2019). Particularly, the outstanding performance in catalysis of it with small size has gained tremendous interests, especially in the catalytic reduction of 4-NP (Fu et al., 2017; You et al., 2017). In this case, the high toxic 4-NP, one kind of “Priority Pollutant” listed by the USEPA, is efficiently converted to less toxic 4-aminophenol (4-AP) under mild reaction conditions, which reduces the risk of environmental pollution (Soğukömeroğulları et al., 2019; Fu et al., 2019a). On the other hand, the product of 4-AP plays important industrial roles on the preparation of drugs, dyes, corrosion inhibitors, and photographic developers, which brings huge economic benefits (Zhou et al., 2018). However, colloidal AuNPs are easy to aggregate because of its high surface energy and always need protective agent in the preparation process (Lai et al., 2017; Qiao et al., 2017; Lai et al., 2015). It is obvious that the catalytic activity will be limited and the energy consumption will increase. Thus, it is necessary to develop an effective way to retain the high dispersity and catalytic activity of AuNPs.

With this respect, heterogeneous Au catalysts have been developed (Cho, 2003). The reusability of AuNPs has also been improved. Simultaneously, how to further enhance the catalytic activity has become another topic. In this case, previous reports proposed some feasible approaches: (1) decrease the particle size and narrow the size distribution to improve the catalytic activity (Barrett et al., 2016; Guo et al., 2016); (2) introduce bimetallic or multi-metallic NPs to make use of the synergetic effect generated by these metals (Song et al., 2015; Xiao et al., 2016); (3) introduce porous structure to restrict AuNPs and enhance the adsorption of 4-NP (Sahoo et al., 2015). Porous carbon materials are good candidates because of their excellent adsorption capacity, good thermal and chemical stability, and admirable mechanical properties (Huang et al., 2018; Xiong et al., 2019; Lai et al., 2018; Zhou et al., 2019). Among them, hierarchical porous carbon black (CB), like Vulcan XC-72, has been widely used for the supports, sensors, energy storage or commercial applications due to the advantages of turbostratic structures with high surface area and conductivity, excellent chemical and mechanical stability (Zeng et al., 2018; Chen et al., 2017; Ali et al., 2017; Zhang et al., 2019). Particularly, its properties of low cost and easy availability provide alternative for cost reduction. Besides, there are also many papers have investigated the electrochemical performance of CB-supported metal NPs (Hameed and El-Sherif, 2015). However, to our knowledge, few of them have mentioned the catalytic reduction of nitroaromatics by CB-supported catalysts in the presence of $NaBH_4$.

It is reported that pristine CB is difficult to anchor metal ions or metal NPs because of the low content of oxygen-containing groups on the surface (Xia et al., 2018; Xia et al., 2016). Therefore, most of papers have investigated the property of modified CB via acidification or doping (Hou et al., 2018; Zhao et al., 2014). Nevertheless, investigation on the performance of pristine CB as support is also interesting. Because pristine CB is easy to aggregate and there are abundant pore structures in CB in spite of pristine CB contains low content of oxygen-containing groups, which might be beneficial to restrict the growing of AuNPs in the pore. In addition, aggregated CB may provide hierarchical porous structure, including micro, meso and macro pores, which result in large surface to volume ratio, reduced diffusion resistance, and enhanced transport diffusion (Ng et al., 2018). Thus, smaller AuNPs can be dispersed in CB, the activity, stability and usability would be enhanced also. In addition, CB can provide strong adsorption ability of CB for nitrophenols and dyes due to the π–π stacking interaction and abundant pore structures. The fast electron transfer from CB to AuNPs may cause higher local electron densities and hence enhance the uptake of electron by nitrophenols and dyes. The catalytic activity of Au/CB may can be improved either. Therefore, it is of great importance to investigate the property of pristine CB as support for Au catalyst and the contribution of pore structures to that of the catalytic activity.

In this study, CB restricted Au catalyst was prepared by a simple polyols method, which using ethylene glycol (EG) as the dispersing agent of CB and reducing agent of AuNPs. The reduction of 4-NP by $NaBH_4$ was employed as a model reaction to investigate the catalytic performance of Au/CB catalyst. As comparison, three kinds of typical and well-investigated porous carbon materials, including multi-walled carbon nanotubes (MWCNTs), Activated Cokes (ACk), and activated carbon (AC) were used to anchor AuNPs (Au/C) for the reduction of nitroaromatics. Various technologies, including transmission electron microscopy (TEM), X-ray diffraction (XRD), X-ray photoelectron spectroscopy (XPS), Fourier transform-infrared spectroscopy (FT-IR), scanning electron microscopy (SEM), inductively coupled plasma optical emission spectrometer (ICP-OES), N_2-Brunauer–Emmett–Teller (BET), and Electron paramagnetic resonance (EPR), were used to characterize the property of these catalysts and to gain insight into the mechanism of the catalytic reaction. The crystalline structure of the prepared Au/CB catalyst before and after reaction was characterized either. The universality and real water application of as-prepared Au/CB were further proposed.

2. Experimental section

2.1. Preparation of carbon supported Au catalyst

Preparation of Au/CB catalyst was accomplished using the polyols method (Navalon et al., 2013). Typically, 200 mg of commercial Vulcan XC-72 CB was suspended in 80 mL of EG and sonicated for 30 min. EG served as dispersant and reducing agent. Afterwards, the mixture was heated up to 85 °C under regular vigorous stirring and a moderate amount of $HAuCl_4$ solution ($10\ g{\cdot}L^{-1}$) was added to achieve the required Au loading (from 0.5 to 2.5 wt %). The mixture was further stirred for 4 h to obtain AuNPs and then filtrated and washed by water and ethanol for several times. Finally, the as-prepared catalyst was dried in an oven at 60 °C before use. Other carbon supported Au catalysts including Au/ACk, Au/AC, and Au/MWCNTs were prepared with the same procedure.

2.2. Catalytic reduction performance

To investigate the catalytic activity of prepared Au/C catalysts, reduction of phenols and azo dyes with $NaBH_4$ was performed. All the catalytic process were proposed as the procedure of 4-NP reduction by Au/CB. Firstly, 50 mL of 4-NP (0.5 mM) was freshly prepared and 10 mg of aforementioned catalyst was added under continuous stirring for 1 h to achieve the adsorption-desorption equilibrium. Then, different amount of $NaBH_4$ (the molar amount is 100, 200, 250, 300, 350, 400

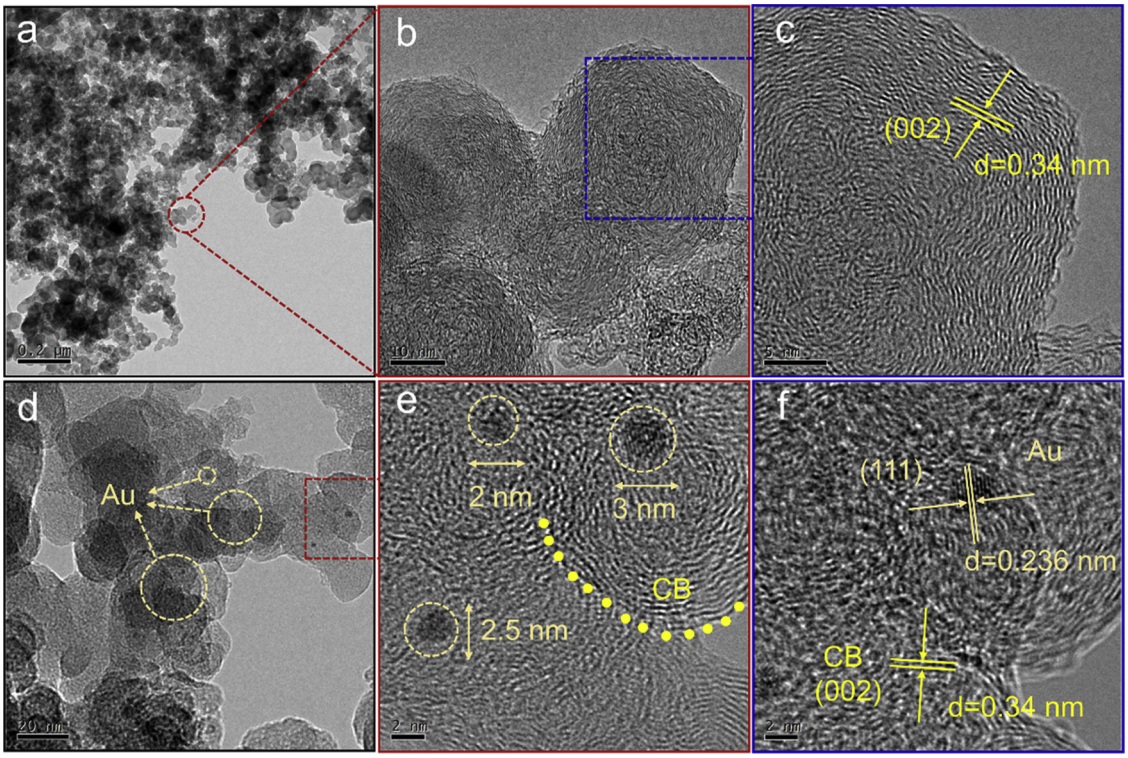

Fig. 1. TEM and HRTEM images of CB (a–c) and Au/CB catalyst (d–f).

times over 4-NP, respectively) was added into the mixture with stirring. The catalytic progress was evaluated by taking 1 mL of the reaction mixture at specified time intervals and diluted five times with ultrapure water. The diluted reaction mixture was measured by UV–vis spectrometry. After reaction, the catalysts were removed by filtration and washed with water and ethanol, then reused for 10 times. The catalytic performance of Au/CB on real water, including bottled water, tap water, lake water, and river water (collected from convenience store, our laboratory, Lake of Peach, and Hsiang River (Changsha, China), respectively), was carried out. The catalytic progress was performed as the reduction of 4-NP in ultrapure water. All the results were achieved by three parallel experiments.

3. Results and discussion

3.1. Characterization of Au/CB catalyst

The morphology and microstructure of pure CB and Au/CB catalyst were verified by the TEM characterization. As shown in Fig. 1a and b, CB has a typically spherical morphology with the size about 30 nm and tends to aggregate because of the high surface energy and van der Waal's forces (Hou et al., 2018). The crystal plane (002) of graphite with a lattice space of 0.34 nm is marked with yellow lines in Fig. 1c, which represents plane between two single graphene layers in CB (Bagavathi et al., 2016). The analysis of the as-synthesized Au/CB catalyst shows that AuNPs are uniformly dispersed on CB with the average size of 2.5 nm (Fig. 1d–f). The high resolution TEM image exhibited in Fig. 1f clearly suggests a lattice of AuNPs with a space of 0.236 nm that can be attributed to the (111) plane of AuNPs, which indicates the successful deposition of AuNPs.

The comparison of XRD analysis for CB and Au/CB catalyst before reaction and after several cycles is depicted in Fig. 2. It is observed that the characteristic peaks in the pattern of CB at 25.0° (d = 0.36 nm) and 43.2° (d = 0.20 nm) are attributed to the (002) and (101) plane reflection of carbon materials. After deposition of AuNPs, the well-defined diffraction peaks of Au/CB located at 38.3, 44.4, 64.6, 77.6, and

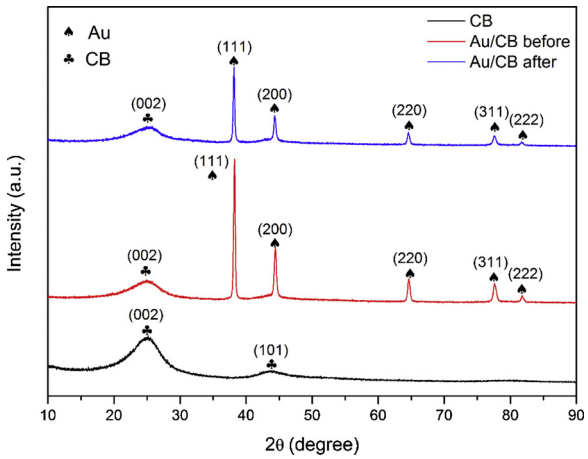

Fig. 2. XRD plots of CB, Au/CB 1.2 wt% catalyst before and after catalytic reduction reaction.

81.8° are indexed to the (111), (200), (220), (311), and (222) crystal plane reflections of Au (JCPDS 04-0784), respectively. However, the characteristic peak of (002) reflection is broad and weak and that of (101) plane disappears. This is because the deposition of AuNPs weakens the internal structure order of CB. This also proves the successful deposition of AuNPs in CB. Meanwhile, after several cycles, all of the crystal plane reflections of Au still exist, but the intensity of peaks has decreased. This implies there may be some AuNPs losing after several reaction cycles.

The XPS spectra of CB, Au/CB, and Au/CB after several cycles were used to determine the elemental composition and chemical state of them. As illustrated in Fig. 3a, the XPS survey spectra demonstrate that there were C and O as the primary elements. The contents of O were very low and the Au in Au/CB before and after several cycles was unconspicuous. While in Fig. 3b, the high-resolution spectra for Au 4f of them are measured. The Au $4f_{7/2}$ and $4f_{5/2}$ peaks are observed at 84.7,

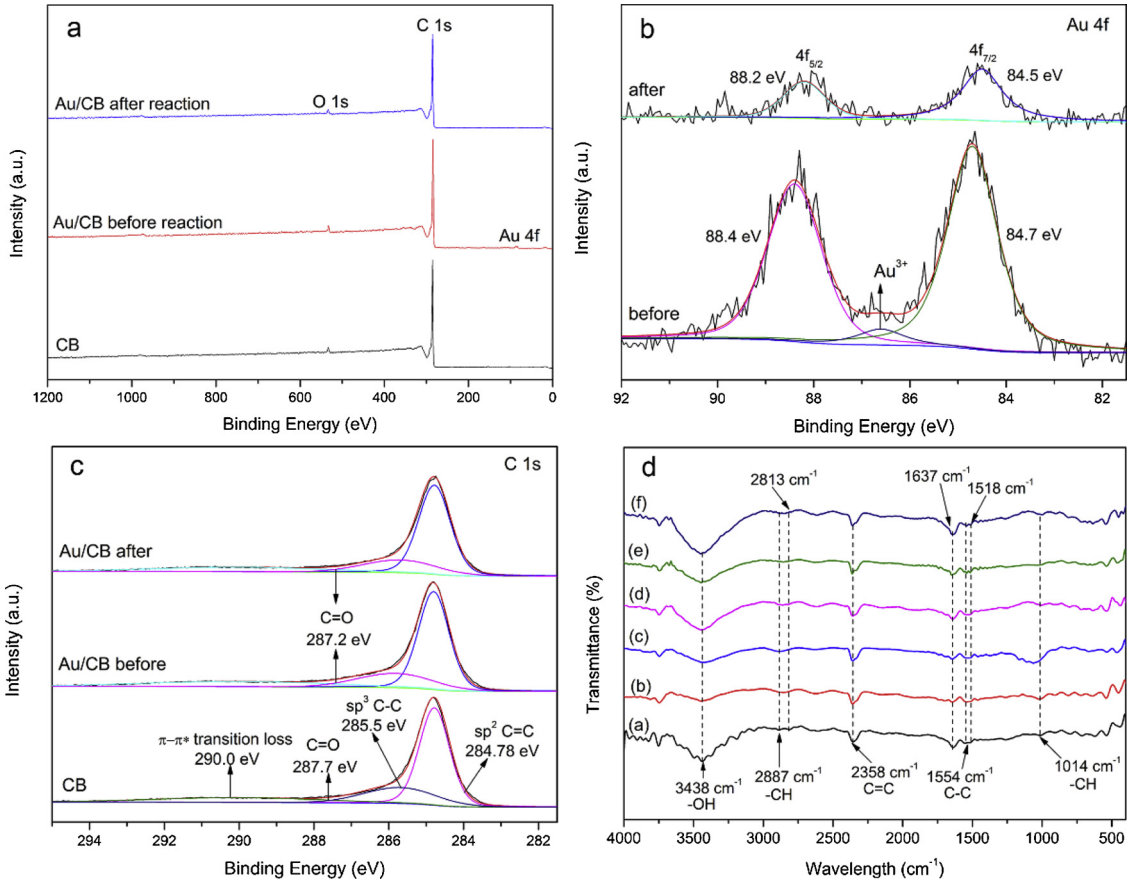

Fig. 3. XPS survey spectra (a), high-resolution spectra for Au 4f (b), and C 1s (c) of CB, Au/CB 1.2 wt% before catalytic reduction reaction and after several cycles. (d) Characteristic FT-IR spectra of CB (inset a) and Au/CB catalyst with different Au loadings (0.4, 0.88, 1.20, 1.34, and 1.39 wt% inset b–f).

88.4, 84.5, and 88.2 eV of Au/CB before and after several cycles respectively, which are typical values of Au in zero oxidation state (Fu et al., 2019b). Besides, a new peak at 86.6 eV assigned to the Au(III) oxidation state in Au/CB before catalytic reaction is observed. This may be because cationic Au species were formed and stabilized on the surface of CB by hydroxyl groups for the formation of Au-O interfacial bonds (Zhao et al., 2018). After reaction, the intensity of Au $4f_{7/2}$ and $4f_{5/2}$ peaks are much lower than that of the one before reaction. This may be because the part of AuNPs on the surface of CB were lost after several cycles. The fitted C 1s spectra of them are exhibited in Fig. 3c. The peaks at 284.78, 285.5 and 290.0 eV are assigned to the sp^2, sp^3 carbon and π-π* transition loss of CB, respectively. The peaks located at 287.7 eV of CB and 287.2 eV of Au/CB are attributed to the C═O, but the content is low.

The characteristic FT-IR spectra of CB and Au/CB catalyst with different Au loadings are shown in Fig. 3d. They all show a series of peaks at about 1014, 2813 and 2887 cm^{-1}, corresponding to the stretching vibration and bending vibration of C–H from the alkane group. The peaks at 1518, 1554, and 1637 cm^{-1} are assigned to the C—C stretching vibration. The rest peaks located at about 2358 and 3438 cm^{-1} are responsible for the C═C stretching vibration and O—H stretching vibration of the hydroxyl group. However, although AuNPs do not show a characteristic absorption band in the FT-IR spectrum, the peak of O—H stretching vibration of Au/CB is smoother than CB and stronger and stronger with the increase of Au loadings, which indicates the strong interaction of Au and CB (Lu et al., 2017).

The nitrogen adsorption-desorption isotherms and pore size distribution of CB and Au/CB 1.2 wt% in the range of micropore, mesopore and macropore are showed in Fig. 4a and b. All apparent curves follow the typical IUPAC type IV pattern with a H_3 hysteresis, suggesting the presence of mesopores and macropore. Interestingly, the BJH pore size distribution further reveals that the main pore size contributions of them are macropores of 108.61 and 114.38 nm (Fig. 4b). In addition, the micropore pore size distribution suggests that there are also micropores and the main micropore size contributions are 0.73 and 0.75 nm for CB and Au/CB (inset of Fig. 4b). According to the TEM analysis, the pore of dispersed CB is micropore. Hence, the mesopores and macropore in CB may be because of the aggregation of dispersed CB. Interestingly, the main size contribution of CB is changed from micropore to macropore after the deposition of AuNPs. The calculated porous properties of CB and Au/CB with different Au loadings are summarized in Table S1. Results indicated that there were distinct hierarchical porous structures in them. Large specific surface area and hierarchical porous structure were beneficial for the adsorption of organic molecules, resulting in improved catalytic performance of Au/CB. Furthermore, the deposition of Au decreased the specific surface area, pore volume, and average pore size, indicating the pores of CB were blocked by Au. It is reasonable to suppose that AuNPs were restricted in the porous channel of CB.

3.2. Catalysis properties of Au/CB

The catalytic performance of as-prepared Au/CB catalysts was explored in the catalytic reduction of 4-NP by $NaBH_4$ as a model reaction at ambient temperature. The absorption peak of 4-NP in the UV–vis spectra located at 317 nm, and shifted at 401 nm in the presence of $NaBH_4$ (Fig. S1). The color also changed from light yellow to bright yellow with the addition of $NaBH_4$ and it did not change even for a month (inset of Fig. S1). This change is because of the formation of nitrophenolate ions in the alkaline medium of $NaBH_4$, which confirms

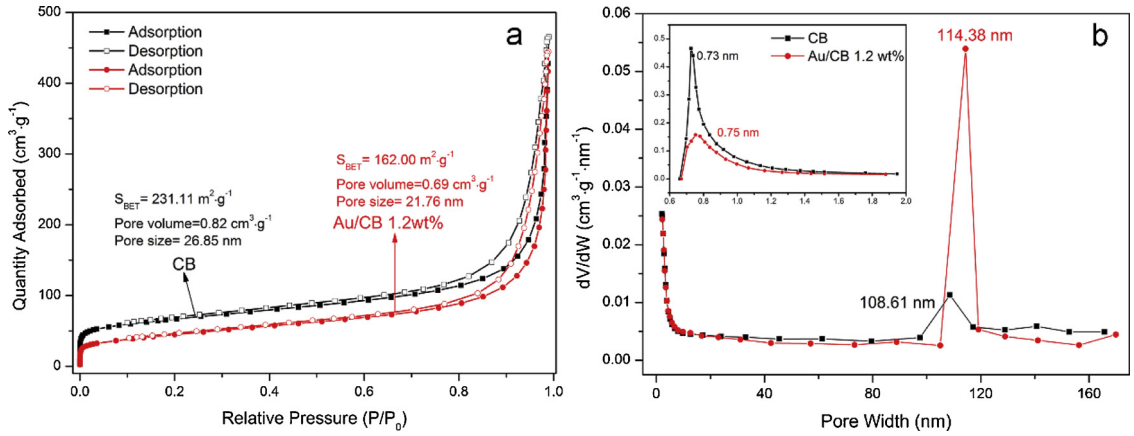

Fig. 4. Nitrogen adsorption-desorpton isotherms (a), BJH pore size distribution (b), and micropore pore size distribution (inset of b) of CB and Au/CB 1.2 wt% catalyst.

that the catalytic reduction was not triggered when only $NaBH_4$ was present. However, with the addition of a small amount of Au/CB (0.2 g L^{-1}), the absorption peak of 4-NP decreased and a new peak at 301 nm increased subsequently. The color changed from bright yellow to colorless, suggesting the production of 4-AP. During the whole reduction process, the amounts of $NaBH_4$ were much higher than that of 4-NP. Hence, the pseudo-first order kinetics can be used to describe the reduction process (Qin et al., 2019a). The performance of as-prepared catalysts can be evaluated by the apparent rate constants (k_{app}) according to Eq. (1) (Que et al., 2015).

$$k_{app} = -\ln (C_t/C_0)/t \quad (1)$$

where C_0 and C_t are the concentration of 4-NP at the initial time and different reaction time (t), they can be replaced with the absorbance of 4-NP (namely A_0 and A_t). In this respect, the catalytic performance of different Au loadings was investigated. The corresponding k_{app} for Au/CB with different Au loadings are listed in Table S2.

It is worth noting that the calculated loadings of Au are 0.5, 1.0, 1.5, 2.0, and 2.5 wt% respectively. However, the measurement contents of them by ICP-OES are 0.4, 0.88, 1.2, 1.34, and 1.39 wt%, which are lower than the theoretical values. One of the reason may consist in the relatively low amount of oxygen-containing groups in CB, which limits the ability to anchor metal NPs on the surface (Ali et al., 2017). With the increase of Au amount, the deposition sites of CB are plateaued, leading to the loss of AuNPs. Another possible reason is that AuNPs are reduced partially, resulting from the loss of $HAuCl_4$. In any case, with the increase of Au loadings, the catalytic activity of Au/CB is increased. Au/CB with 1.2 wt% exhibits the highest catalytic activity with the k_{app} of 0.8302 min^{-1} (Fig. 5). As the loadings increase sequentially, the activity of Au/CB tends to decrease inversely. It is possibly because larger amount of AuNPs reduced the porous channel of CB, decreasing the specific surface area, pore size, and pore volume of catalyst, thus limiting the adsorption of 4-NP (Table S2). In addition, the turnover frequency (TOF) of Au/CB with different Au loadings was further calculated to evaluate the catalytic efficiency of as-prepared Au/CB catalysts. As exhibited in Table S2, the TOF of Au/CB with 1.2 wt% loading is much higher (492.50 h^{-1}) than the others, implying it exhibits better catalytic performance compared to the other loadings. Besides, this work shows good catalytic performance when compared with other previous reports (Table S3).

It is necessary to investigate the effect of $NaBH_4$ concentration because this reduction reaction was triggered by $NaBH_4$. To investigate the influence on catalytic performance with different amounts of $NaBH_4$, the molar amount of $NaBH_4$ for 100, 200, 250, 300, 350, and 400 times over 4-NP was added to trigger the catalytic reduction. As indicated in Fig. S2, the k_{app} increased significantly with the increase of $NaBH_4$. However, over 300 times of $NaBH_4$, the rates of rise reached the maximum because the reactants were saturated and the rate could not be improved even with more $NaBH_4$. This phenomenon is similar to the reported paper (Gupta et al., 2014). Hence, in this paper, the concentration of $NaBH_4$ was chosen as 300 times over the amount of 4-NP, namely 150 mM.

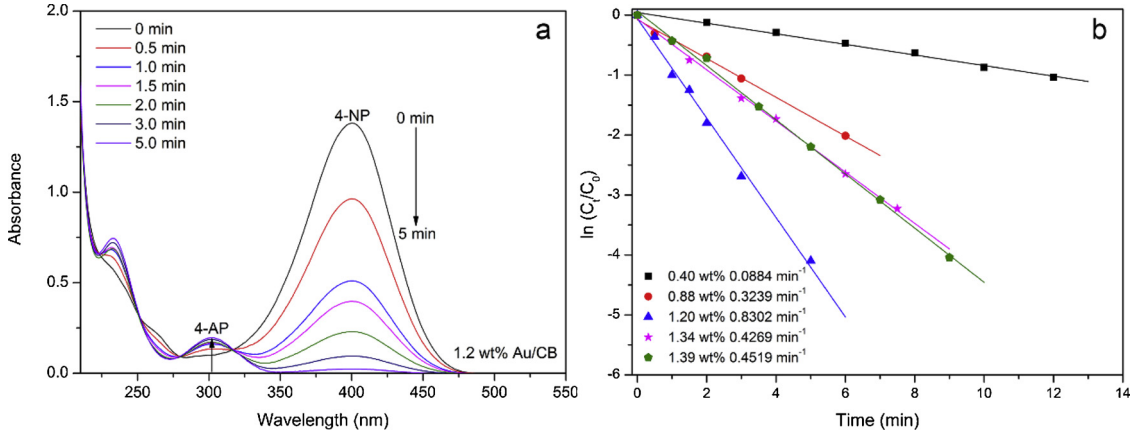

Fig. 5. Time-dependent UV–vis absorption spectra of 4-NP catalyzed by Au/CB 1.20 wt% catalyst (a). Plots of ln(C_t/C_0) versus reaction time and pseudo-first-order kinetics fitting of Au/CB with different Au catalysts (b).

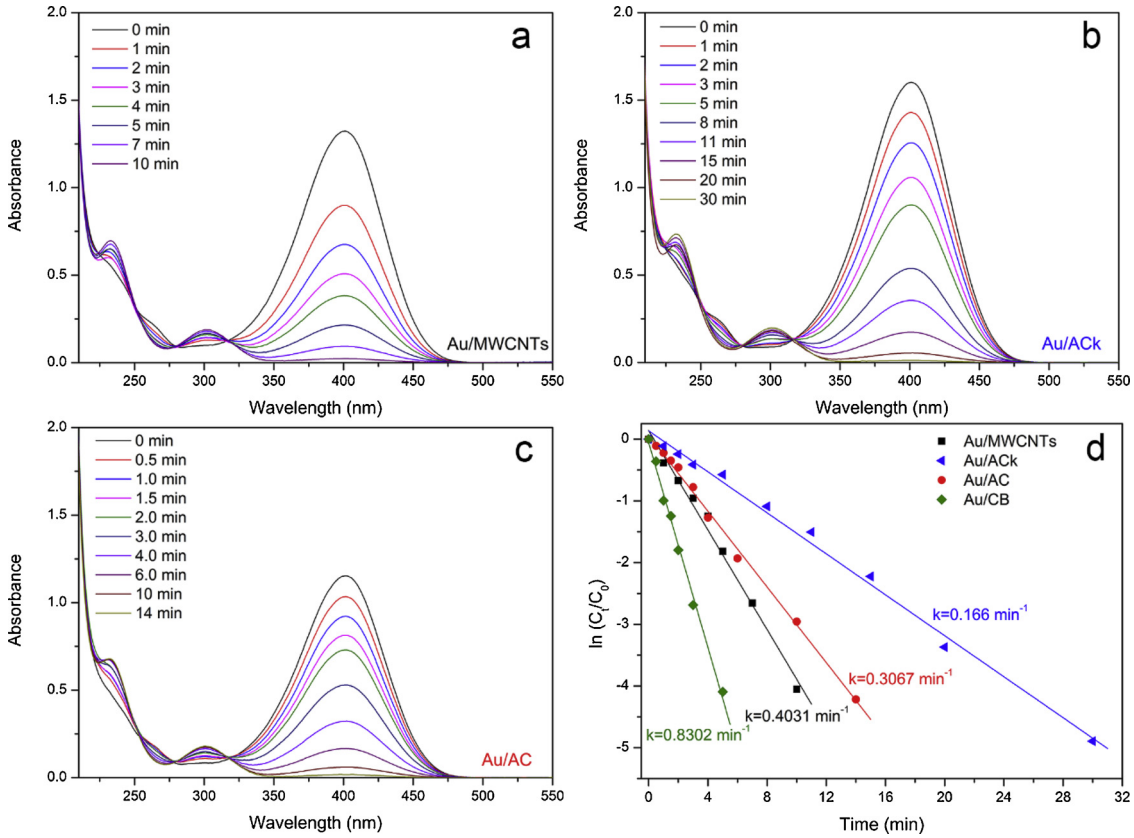

Fig. 6. Time-dependent UV–vis absorption spectra of 4-NP catalyzed by Au/MWCNTs (a), Au/ACk (b), and Au/AC (c). Plots of pseudo-first-order kinetics fitting by Au/MWCNTs, Au/ACk, Au/AC, and Au/CB (d).

3.3. Catalytic performance of other Au/C catalysts

ACk and AC are both biomass charcoals with abundant porous structure and huge specific surface area. MWCNTs are widely used in environmental remediation. In order to explore the performance of porosity on Au catalysts for catalytic reduction, these four kinds of porous carbon materials were employed as supports to anchor AuNPs. The reduction of 4-NP by these catalysts were also proposed as comparison. The UV–vis spectra and pseudo-first-order kinetics fitting plot at suitable intervals are illustrated in Fig. 6. With the addition of catalysts, 4-NP was reduced completely about 10, 30, and 14 min for Au/MWCNTs, Au/ACk, and Au/AC respectively. As expected, the catalytic activity of Au/CB is much higher than the others and the reducing rates follow the order of Au/CB > Au/MWCNTs > Au/AC > Au/ACk with the values of 0.8302, 0.4031, 0.3067, and 0.166 min^{-1}. In this case, the XRD of Au/CB, Au/MWCNTs, Au/ACk, and Au/AC was measured as comparison. As shown in Fig. S3a, the characteristic peaks of XRD representing the (111), (200), (220), (311), and (222) crystal plane reflections of Au are observed in all of these catalysts, which means AuNPs were successfully deposited. The peak intensity of Au/CB is higher than the others, contributing to the highest catalytic activity. Interestingly, the peak intensity of Au/AC is higher than Au/MWCNTs, while the catalytic activity of Au/MWCNTs is better. To explain this phenomenon, the TEM of them was further measured. As obviously observed in Fig. S3b–d, AuNPs are successfully deposited on MWCNTs, ACk, and AC, but the AuNPs in Au/AC are aggregated obviously. It is reported that the catalytic activity of AuNPs were higher with the smaller particle size when the loading amount was the same (Panigrahi et al., 2007). Thus, the aggregated AuNPs in Au/AC drastically decreased the catalytic activity. Besides, the particles are well dispersed in Au/MWCNTs and the size of AuNPs in it about 5 nm is much smaller than the others. Thus, it is reasonable that the catalytic activity of Au/MWCNTs is higher than Au/AC and Au/ACk. Even so, it is important to remark that the catalytic activity of Au/MWCNTs is still lower than Au/CB because the size of AuNPs in Au/CB is smaller than Au/MWCNTs. On the other hand, the BET surface area of MWCNTs is about 110 $m^2 g^{-1}$, which is much smaller than CB, hence limiting the adsorption of 4-NP and further decreasing the catalytic activity.

3.4. Test of universality, stability, and practical application

In order to illustrate the universality of Au/CB catalyst, the catalytic reduction of other typical phenols and azo dyes, including 2-nitrophenol (2-NP), 3-nitrophenol (3-NP), 2, 4-dinitrophenol (2, 4-DNP), Congo red (CR), methyl orange (MO), and Erichrome Black T (EBT), by Au/CB with 1.2 wt% loading was also proposed with the same procedure of 4-NP reduction. The UV–vis spectra and pseudo-first-order kinetics fitting parameters of them are provided in Fig. 7 and Table S4. The results suggest that these compounds can be well reduced and the catalytic rate follows the order of MO > 4-NP > 2-NP > 3-NP > 2, 4-DNP > EBT > CR with catalytic rates of 1.2869, 0.8302, 0.4599, 0.4459, 0.4287, 0.4085, and 0.3652 min^{-1}, respectively. The results are highly corresponded with the reported papers (Xia et al., 2016; Qin et al., 2019b). It also demonstrates that this Au/CB catalyst can be used widely. Interestingly, the 2, 4-DNP with $NaBH_4$ shows two absorption peaks at about 258 and 360 nm in the UV–vis spectrum. The two peaks at 258 and 360 nm decrease gradually with the addition of Au/CB and two new peaks appear at 276 and 442 nm, which indicates the formation of 2, 4-dinitrophenolate intermediate. With the further increasing of reaction time, the peak at 442 nm decreases and a new peak at 300 nm appears. The color of 2, 4-DNP also changes from yellow to pale orange and colorless during the whole reaction process. These results indicate the formation of 2, 4-diaminophenol and are in well agreement with the previous reports (Gerelbaatar et al., 2018; Karakas et al.,

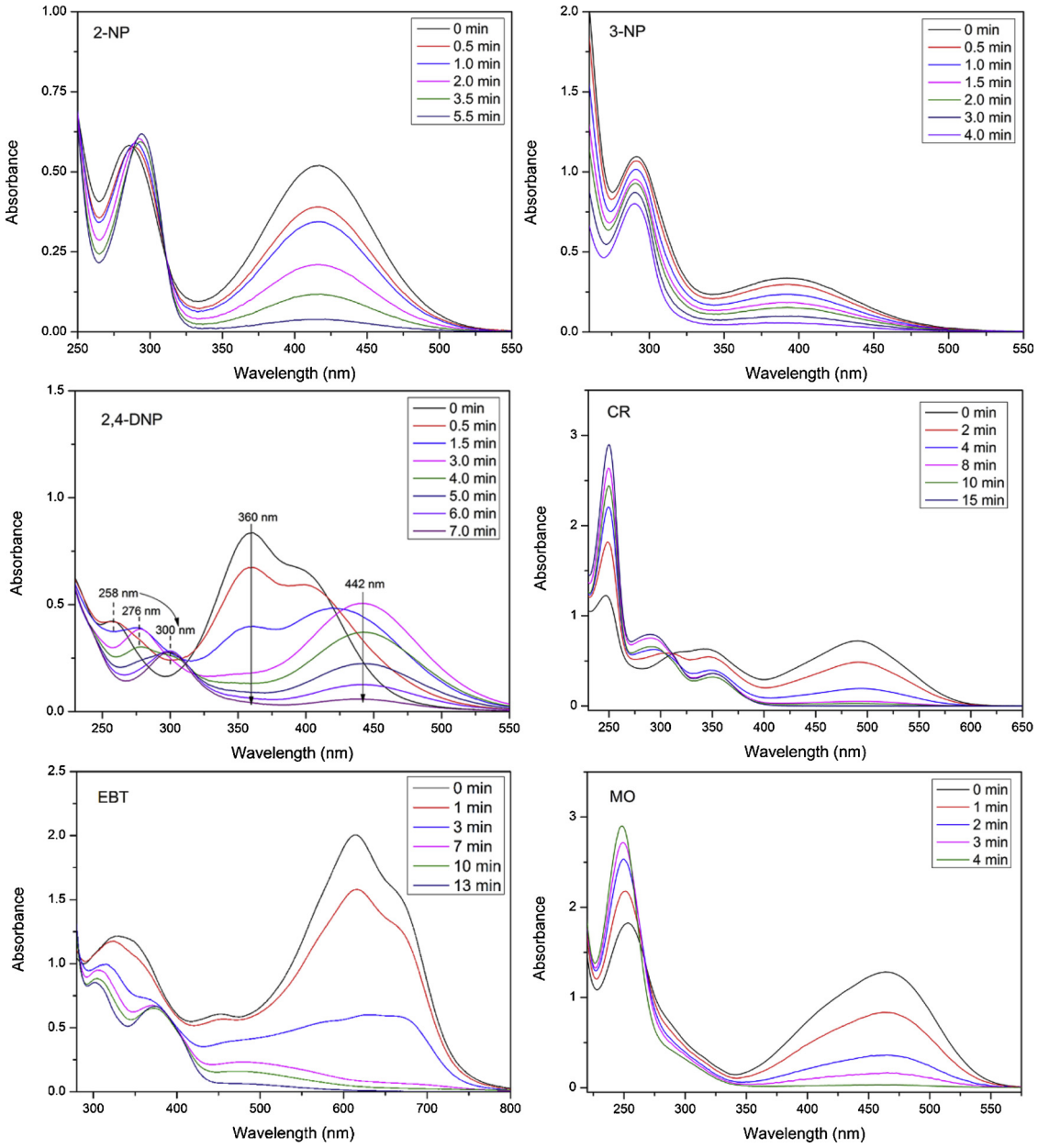

Fig. 7. Time-dependent UV–vis absorption spectra of 2-NP, 3-NP, 2, 4-DNP, CR, EBT, and MO reduced by Au/CB catalyst.

2017).

To investigate the stability and reusability, the Au/CB was reused to reduce 4-NP about 10 cycles. As exhibited in Fig. 8, the Au/CB shows continuous decrease of catalytic activity within the first several re-cycles, but still reveals a high catalytic efficiency of 4-NP reduction. After the third cycle, the activity of Au/CB tends to be stable. It may be because the loss of AuNPs on the surface decrease the catalytic activity, while the AuNPs inside remain stable catalytic activity for 4-NP reduction. Combining the results of XPS and XRD for Au/CB before and after several cycles, we speculate that AuNPs on the surface may be easy to loss but AuNPs restricted in the pore channels are stable and can provide good catalytic activity.

On the other hand, the catalytic performance on real water samples is very important. On this basis, reduction of 4-NP by Au/CB with 1.2 wt% loading on bottled water, tap water, lake water, and river water was performed. Obviously, 4-NP can eventually be completely reduced in these samples (Fig. 9), and the catalytic rates are 0.4480, 0.3613, 0.2800, and 0.1303 min^{-1} for river water, bottled water, lake

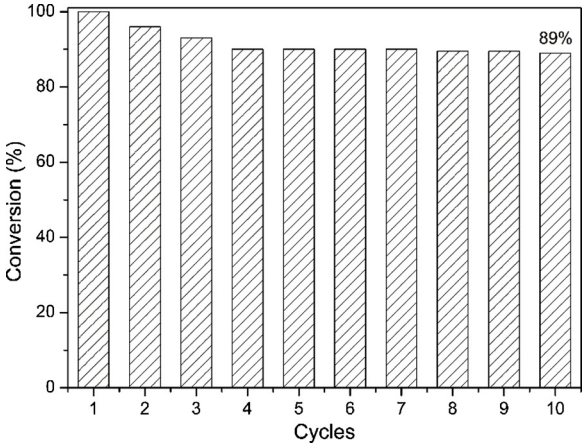

Fig. 8. Reusability of 4-NP reduction by Au/CB for 50 min over 10 cycles.

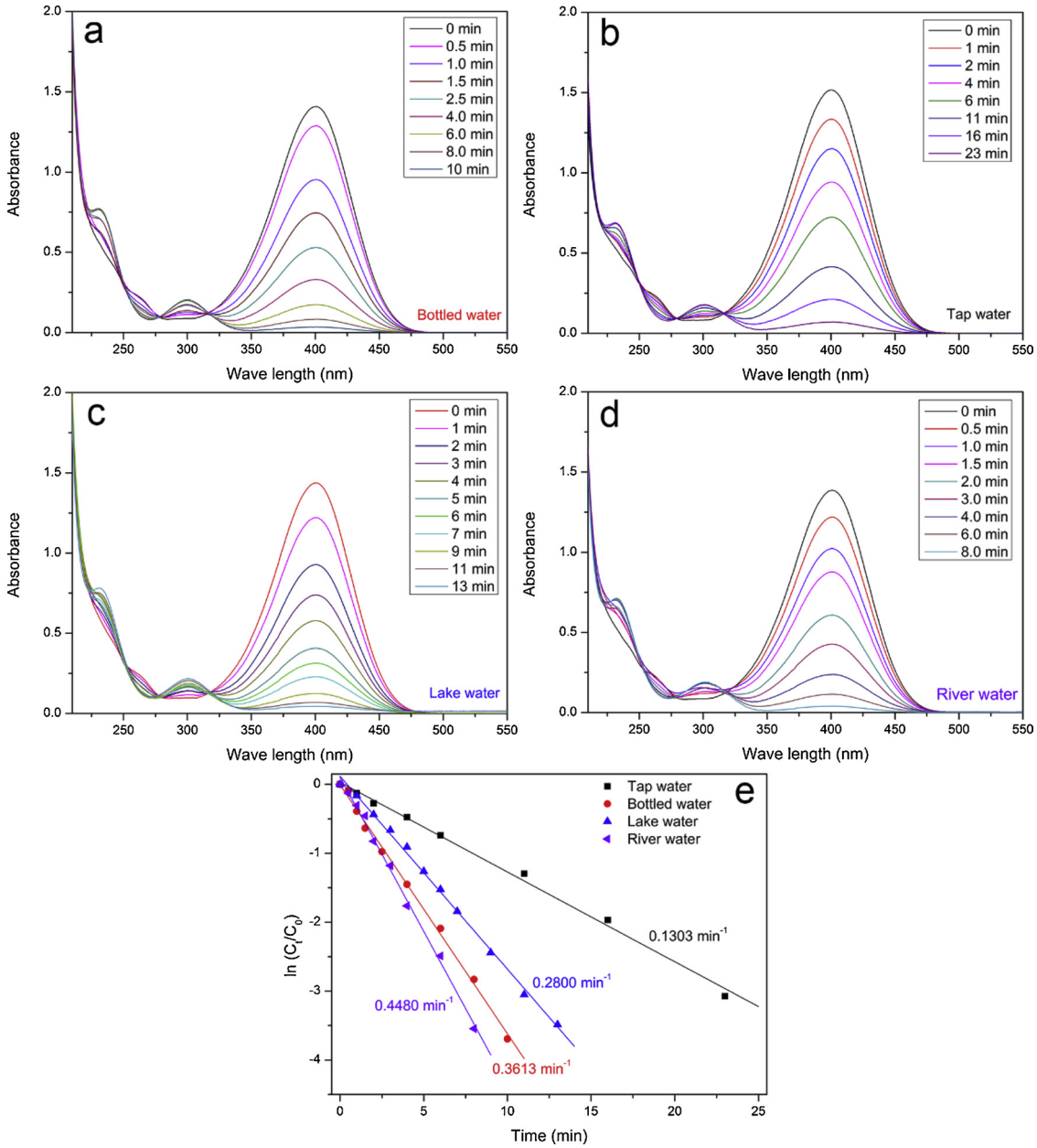

Fig. 9. Time-dependent UV–vis absorption spectra of 4-NP reduction by Au/CB on bottled water (a), tap water (b), lake water (c), and river water (d) and the pseudo-first-order kinetics fitting plots of them (e).

water, and tap water, in which the catalytic activity on tap water is the lowest one. This is possible because there are disinfectants or plenty of dissolved oxygen (DO) which can consume $NaBH_4$, leading to limited catalytic activity. In this case, the concentration of ClO^-, Cl^-, and DO in these samples were detected. As shown in Table S5, the concentrations of ClO- and DO in tap water are higher than the others, especially the ClO^- is not found except in the tap water. This results verify the speculation that the catalytic activity of Au/CB in real water is highly connected with the concentration of ClO^- and DO. However, the concentration of DO in lake water is the lowest, but the activity is lower than the river water. This may be because of the presence of Cl- in lake water, which will poison the catalyst, thus reducing the catalytic efficiency. Anyway, the results for real water application reveal that the prepared Au/CB catalyst has great potential for practical application.

3.5. Mechanistic insight in the reduction of nitroaromatics by Au/CB system

Dispersed CB is spherical but easy to aggregate. According to the above analysis, we speculated that some CBs were aggregated, resulting in the formation of macropore and mesoporous. Most of AuNPs were restricted inside the pores of CB. To verify this speculation, the SEM images with EDS analysis of Au/CB catalyst were proposed. As observed from Fig. S4, most of elements on the surface of Au/CB are C and O, while a very small part is Au. In addition, Au is not even detected in some places. The low content of AuNPs on the surface of Au/CB catalyst is similar with the results of XPS. However, the XRD analysis showed relatively strong diffraction peaks of AuNPs in Au/CB. The TEM images also demonstrated the presence of dispersed AuNPs. Hence, the possible mechanism of this reaction is proposed. Due to the excess use of $NaBH_4$ and the calculation of pseudo-first order kinetics, the mechanism of this reaction can be proposed as the Langmuir–Hinshelwood model. As shown in Scheme 1 , when nitroaromatics added in the system, they are

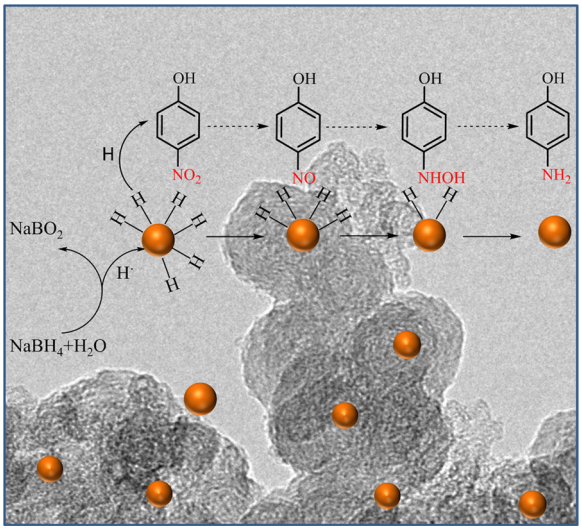

Scheme 1. Mechanism of catalytic reduction of 4-NP by Au/CB catalyst before reaction and after several cycles.

rapidly absorbed on the surface of CB because of the π-π stacking interaction, which promoting the access of nitroaromatics to AuNPs. In addition, the strong electron-withdrawing ability of nitro-group in nitroaromatics further enhances the π-π stacking interaction between nitroaromatics and CB (Liu et al., 2010). As the presence of $NaBH_4$, it reacts with water and plenty of activation hydrogen (i.e. H˙ radical species) is released. Subsequently, AuNPs capture the H˙ radical species to form Au-H bond. Due to the electronegativity discrepancy between H˙ and Au, positively charged N in the nitro-group of nitroaromatics is attacked by H˙. The nitro-group is successfully reduced to nitroso group, hydroxylamine, and finally turns into the corresponding products. To verify the formation of Au-H bond and identify the role of AuNPs, EPR with 5, 5-Dimethylpyrroline N-oxide (DMPO) as a spin trapper was proposed to explore the evolution of H˙ radical species. As shown in Fig. S5a, a high signal intensity of nine-line SPR spectra is observed when DMPO presents in the solution containing $NaBH_4$, 4-NP + $NaBH_4$, and 4-NP + $NaBH_4$ + Au/CB 1.2 wt%. These spectra are composed by a 1:1:1 triplet of 1:2:1 triplets with a_N = 16.62 G and a_H = 22.58 G, which means there are plenty of H˙ radical adducts in the solutions. Simultaneously, no signal is observed in the absence of $NaBH_4$, which indicates H˙ radical adducts are mainly produced by $NaBH_4$. Nevertheless, the intensity of H˙ radical adducts is higher when Au/CB is added. This suggests the presence of Au/CB can promote the generation of H˙ radical adducts and form the Au-H bond (Abad et al., 2005; Nguyen et al., 2019). Moreover, the evaluation of H˙ radical adducts with time change was also detected (Fig. S5b). At the beginning of reaction, $NaBH_4$ is the main resource of H˙ radical adducts. The intensity of H˙ radical adducts trends to be stable. With time changes, the intensity increases and finally decreases, which indicates the consumption of H˙ radical adducts and completion of catalytic reduction. Since the reduction takes place on the active sites of AuNPs, the reduction process is a cycle of H˙ radical adducts trap and transportation.

In this study, AuNPs are deposited both inside and on the surface of CB at the first cycle. The high activity of Au/CB with the content of 1.2 wt% can be attributed to the abundant hierarchical porous structure of CB and the synergistic effect of AuNPs and CB. Firstly, CB has high specific surface area for restricting Au, which is in favor to improve the stability. Secondly, the relatively small size and high dispersion of AuNPs provides more active sites, leading to high catalytic activity. Thirdly, the strong adsorption ability of CB towards phenols and dyes makes a higher concentration of targets near to the AuNPs, resulting in highly efficient contact between the targets and active sites. Most importantly, the property of CB with conductive matrix and supercapacitance promotes the electron transfer from CB to AuNPs, causing higher local electron densities and hence enhancing the uptake of electron by nitroaromatics. Although there are small amount of oxygen-containing groups on the surface of CB, part of AuNPs are still anchored on the surface. However, after several cycles, the surface AuNPs tend to shed from CB and the catalytic activity decreases slightly. Fortunately, there are plenty of AuNPs may be restricted inside of CB because of the abundant porous structure. Therefore, the relatively stable and high activity can be achieved.

4. Conclusion

In order to investigate the property of pristine CB as the support for heterogeneous Au catalyst, an Au/CB catalyst was prepared by a simple polyols method for nitroaromatics reduction. Different kinds of porous carbon materials including CB, ACk, AC, and MWCNTs used as supports to anchor AuNPs were proposed as comparison to explore the contribution of pore structures for the catalytic activity. Results showed that Au/CB exhibited higher activity and lower cost than others. The abundant hierarchical porous structures of CB provided strong adsorption ability of nitroaromatics, which resulted in the high catalytic efficiency. Interestingly, the aggregation of CB provided more pores, which were beneficial for the AuNPs anchoring. The synergistic effect between AuNPs and CB further enhanced the catalytic activity. In addition, this Au/CB catalyst showed good universality, stability, and practical application. The hierarchical porous structures of CB are contributed to the high stable and catalytic activity of Au/CB, and because of the low cost it can be further used in environment field.

Acknowledgments

This study was financially supported by the Program for the National Natural Science Foundation of China (51579098, 51879101, 51779090, 51709101, 51278176, 51408206, 51521006, 51809090, 51378190), Science and Technology Plan Project of Hunan Province (2016RS3026, 2017SK2243, 2018SK20410), Hunan Provincial Innovation Foundation For Postgraduate (CX2018B155), the National Program for Support of Top-Notch Young Professionals of China (2014), the Program for New Century Excellent Talents in University (NCET-13-0186), the Program for Changjiang Scholars and Innovative Research Team in University (IRT-13R17), and the Fundamental Research Funds for the Central Universities (531107050978, 531107051080, 531109200027). The authors would like to thank Xiaobing Zhou from Shiyanjia Lab (www.shiyanjia.com) for the EPR analysis.

Appendix A. Supplementary data

Supplementary material related to this article can be found, in the online version, at doi:https://doi.org/10.1016/j.jhazmat.2019.120864.

References

Abad, A., Conception, P., Corma, A., García, H., 2005. Gold-organic-inorganic high surface-area materials as precursors of highly active catalysts. Angew. Chem. 117, 4134–4137.

Abazari, R., Mahjoub, A.R., Salehi, G., 2019. Preparation of amine functionalized g-C_3N_4@H/SMOF NCs with visible light photocatalytic characteristic for 4-nitrophenol degradation from aqueous solution. J. Hazard. Mater. 365, 921–931.

Abdullah, H., Susanto Gultom, N., Kuo, D.-H., 2019. Synthesis and characterization of La-doped Zn(O,S) photocatalyst for green chemical detoxification of 4-nitrophenol. J. Hazard. Mater. 363, 109–118.

Ai, Y., Hu, Z., Liu, L., Zhou, J., Long, Y., Li, J., Ding, M., Sun, H.-B., Liang, Q., 2019. Magnetically hollow Pt nanocages with ultrathin walls as a highly integrated nanoreactor for catalytic transfer hydrogenation reaction. Adv. Sci. 6, 1802132–1802142.

Ali, F., Khan, S.B., Kamal, T., Anwar, Y., Alamry, K.A., Asiri, A.M., 2017. Bactericidal and catalytic performance of green nanocomposite based-on chitosan/carbon black fiber supported monometallic and bimetallic nanoparticles. Chemosphere 188, 588–598.

Bagavathi, M., Ramar, A., Saraswathi, R., 2016. Fe_3O_4–carbon black nanocomposite as a highly efficient counter electrode material for dye-sensitized solar cell. Ceram. Int.

42, 13190–13198.
Barrett, D.H., Scurrell, M.S., Rodella, C.B., Diaz, B., Billing, D.G., Franklyn, P.J., 2016. Achieving nano-gold stability through rational design. Chem. Sci. 7, 6815–6823.
Chen, Z., Dong, H., Yu, H., Yu, H., 2017. In-situ electrochemical flue gas desulfurization via carbon black-based gas diffusion electrodes: performance, kinetics and mechanism. Chem. Eng. J. 307, 553–561.
Cheng, M., Zeng, G., Huang, D., Lai, C., Liu, Y., Zhang, C., Wang, R., Qin, L., Xue, W., Song, B., 2018. High adsorption of methylene blue by salicylic acid-methanol modified steel converter slag and evaluation of its mechanism. J. Colloid Interface Sci. 515, 232–239.
Cho, A., 2003. Connecting the dots to custom catalysts. Science 299, 1684–1685.
Ciriminna, R., Falletta, E., Della Pina, C., Teles, J.H., Pagliaro, M., 2016. Industrial applications of gold catalysis. Angew. Chem. Int. Ed. 55, 14210–14217.
Fu, Y., Huang, T., Jia, B., Zhu, J., Wang, X., 2017. Reduction of nitrophenols to aminophenols under concerted catalysis by Au/gC_3N_4 contact system. Appl. Catal. B: Environ. 202, 430–437.
Fu, Y., Qin, L., Huang, D., Zeng, G., Lai, C., Li, B., He, J., Yi, H., Zhang, M., Cheng, M., Wen, X., 2019a. Chitosan functionalized activated coke for Au nanoparticles anchoring: green synthesis and catalytic activities in hydrogenation of nitrophenols and azo dyes. Appl. Catal. B: Environ. 255, 117740.
Fu, Y., Xu, P., Huang, D., Zeng, G., Lai, C., Qin, L., Li, B., He, J., Yi, H., Cheng, M., Zhang, C., 2019b. Au nanoparticles decorated on activated coke via a facile preparation for efficient catalytic reduction of nitrophenols and azo dyes. Appl. Surf. Sci. 473, 578–588.
Gerelbaatar, K., Tsogoo, A., Dashzeveg, R., Tsedev, N., Ganbold, E.O., 2018. Reduction of 2,4-dinitrophenol to 2,4-diaminophenol using AuNPs and AgNPs as catalyst. Solid State Phenom. 271, 76–84.
Gong, X., Huang, D., Liu, Y., Zeng, G., Wang, R., Wan, J., Zhang, C., Cheng, M., Qin, X., Xue, W., 2017. Stabilized nanoscale zerovalent iron mediated cadmium accumulation and oxidative damage of Boehmeria nivea (L.) Gaudich cultivated in cadmium contaminated sediments. Environ. Sci. Technol. 51, 11308–11316.
Guo, M., He, J., Li, Y., Ma, S., Sun, X., 2016. One-step synthesis of hollow porous gold nanoparticles with tunable particle size for the reduction of 4-nitrophenol. J. Hazard. Mater. 310, 89–97.
Guo, X., Peng, Z., Huang, D., Xu, P., Zeng, G., Zhou, S., Gong, X., Cheng, M., Deng, R., Yi, H., Luo, H., Yan, X., Li, T., 2018. Biotransformation of cadmium-sulfamethazine combined pollutant in aqueous environments: phanerochaete chrysosporium bring cautious optimism. Chem. Eng. J. 347, 74–83.
Gupta, V.K., Atar, N., Yola, M.L., Üstündağ, Z., Uzun, L., 2014. A novel magnetic Fe@Au core–shell nanoparticles anchored graphene oxide recyclable nanocatalyst for the reduction of nitrophenol compounds. Water Res. 48, 210–217.
Hameed, R.M.A., El-Sherif, R.M., 2015. Microwave irradiated nickel nanoparticles on Vulcan XC-72R carbon black for methanol oxidation reaction in KOH solution. Appl. Catal. B: Environ. 162, 217–226.
Hou, Y., Zhao, T., Shi, Y., Fan, J., Zheng, R., Zhang, Y., Gu, Q., 2018. Surface modification of carbon black to facilitate suspension polymerization of styrene and carbon black. J. Appl. Polym. Sci. 135, 46387.
Hu, Z., Zhou, J., Ai, Y., Liu, L., Qi, L., Jiang, R., Bao, H., Wang, J., Hu, J., Sun, H.-b., Liang, Q., 2018. Two dimensional Rh/Fe_3O_4/g-C_3N_4-N enabled hydrazine mediated catalytic transfer hydrogenation of nitroaromatics: a predictable catalyst model with adjoining Rh. J. Catal. 368, 20–30.
Huang, D., Deng, R., Wan, J., Zeng, G., Xue, W., Wen, X., Zhou, C., Hu, L., Liu, X., Xu, P., 2018. Remediation of lead-contaminated sediment by biochar-supported nano-chlorapatite: accompanied with the change of available phosphorus and organic matters. J. Hazard. Mater. 348, 109–116.
Karakas, K., Celebioglu, A., Celebi, M., Uyar, T., Zahmakiran, M., 2017. Nickel nanoparticles decorated on electrospun polycaprolactone/chitosan nanofibers as flexible, highly active and reusable nanocatalyst in the reduction of nitrophenols under mild conditions. Appl. Catal. B: Environ. 203, 549–562.
Cui, L., Lei, Q., Guangming, Z., Yunguo, L., Danlian, H., Chen, Z., Piao, X., Min, C., Xiangbin, Q., Manman, W., 2015. Sensitive and selective detection of mercury ions based on papain and 2,6-pyridinedicarboxylic acid functionalized gold nanoparticles. RSC Adv. 6, 3259–3266.
Lai, C., Wang, M.-M., Zeng, G.-M., Liu, Y.-G., Huang, D.-L., Zhang, C., Wang, R.-Z., Xu, P., Cheng, M., Huang, C., 2016. Synthesis of surface molecular imprinted TiO_2/graphene photocatalyst and its highly efficient photocatalytic degradation of target pollutant under visible light irradiation. Appl. Surf. Sci. 390, 368–376.
Lai, C., Liu, X., Qin, L., Zhang, C., Zeng, G., Huang, D., Cheng, M., Xu, P., Yi, H., Huang, D., 2017. Chitosan-wrapped gold nanoparticles for hydrogen-bonding recognition and colorimetric determination of the antibiotic kanamycin. Microchim. Acta 184, 2097–2105.
Lai, C., Liu, S., Zhang, C., Zeng, G., Huang, D., Qin, L., Liu, X., Yi, H., Wang, R., Huang, F., Li, B., Hu, T., 2018. Electrochemical aptasensor based on sulfur–nitrogen codoped ordered mesoporous carbon and thymine–Hg^{2+}–thymine mismatch structure for Hg^{2+} detection. ACS Sens. 3, 2566–2573.
Li, B., Lai, C., Zeng, G., Qin, L., Yi, H., Huang, D., Zhou, C., Liu, X., Cheng, M., Xu, P., Zhang, C., Huang, F., Liu, S., 2018. Facile hydrothermal synthesis of Z-scheme $Bi_2Fe_4O_9$/Bi_2WO_6 heterojunction photocatalyst with enhanced visible light photocatalytic activity. ACS Appl. Mater. Interfaces 10, 18824–18836.
Li, L., Lai, C., Huang, F., Cheng, M., Zeng, G., Huang, D., Li, B., Liu, S., Zhang, M., Qin, L., Li, M., He, J., Zhang, Y., Chen, L., 2019. Degradation of naphthalene with magnetic bio-char activate hydrogen peroxide: synergism of bio-char and Fe–Mn binary oxides. Water Res. 160, 238–248.
Liu, Q.S., Zheng, T., Wang, P., Jiang, J.P., Li, N., 2010. Adsorption isotherm, kinetic and mechanism studies of some substituted phenols on activated carbon fibers. Chem. Eng. J. 157, 348–356.
Liu, X., Huang, D., Lai, C., Zeng, G., Qin, L., Zhang, C., Yi, H., Li, B., Deng, R., Liu, S., Zhang, Y., 2018. Recent advances in sensors for tetracycline antibiotics and their applications. TrAC Trends Anal. Chem. 109, 260–274.
Lu, S., Wang, H., Zhou, J., Wu, X., Qin, W., 2017. Atomic layer deposition of ZnO on carbon black as nanostructured anode materials for high-performance lithium-ion batteries. Nanoscale 9, 1184–1192.
Luo, J., Liu, T., Zhang, D., Yin, K., Wang, D., Zhang, W., Liu, C., Yang, C., Wei, Y., Wang, L., 2019. The individual and Co-exposure degradation of benzophenone derivatives by UV/H_2O_2 and UV/PDS in different water matrices. Water Res. 159, 102–110.
Navalon, S., Sempere, D., Alvaro, M., Garcia, H., 2013. Influence of hydrogen annealing on the photocatalytic activity of diamond-supported gold catalysts. ACS Appl. Mater. Interfaces 5, 7160–7169.
Ng, S.W.L., Yilmaz, G., Ong, W.L., Ho, G.W., 2018. One-step activation towards spontaneous etching of hollow and hierarchical porous carbon nanospheres for enhanced pollutant adsorption and energy storage. Appl. Catal. B: Environ. 220, 533–541.
Nguyen, T.B., Huang, C.P., Doong, R.-a., 2019. Enhanced catalytic reduction of nitrophenols by sodium borohydride over highly recyclable Au@graphitic carbon nitride nanocomposites. Appl. Catal. B: Environ. 240, 337–347.
Panigrahi, S., Basu, S., Praharaj, S., Pande, S., Jana, S., Pal, A., Ghosh, S.K., Pal, T., 2007. Synthesis and size-selective catalysis by supported gold nanoparticles: study on heterogeneous and homogeneous catalytic process. J. Phys. Chem. C 111, 4596–4605.
Qiao, X.-Q., Zhang, Z.-W., Tian, F.-Y., Hou, D.-F., Tian, Z.-F., Li, D.-S., Zhang, Q., 2017. Enhanced catalytic reduction of p-Nitrophenol on ultrathin MoS_2 nanosheets decorated with noble metal nanoparticles. Cryst. Growth Des. 17, 3538–3547.
Qin, L., Zeng, G., Lai, C., Huang, D., Zhang, C., Xu, P., Hu, T., Liu, X., Cheng, M., Liu, Y., 2017. A visual application of gold nanoparticles: simple, reliable and sensitive detection of kanamycin based on hydrogen-bonding recognition. Sens. Actuators B: Chem. 243, 946–954.
Qin, L., Zeng, G., Lai, C., Huang, D., Zhang, C., Cheng, M., Yi, H., Liu, X., Zhou, C., Xiong, W., Huang, F., Cao, W., 2019a. Synthetic strategies and application of gold-based nanocatalysts for nitroaromatics reduction. Sci. Total Environ. 652, 93–116.
Qin, L., Huang, D., Xu, P., Zeng, G., Lai, C., Fu, Y., Yi, H., Li, B., Zhang, C., Cheng, M., Zhou, C., Wen, X., 2019b. In-situ deposition of gold nanoparticles onto polydopamine-decorated g-C_3N_4 for highly efficient reduction of nitroaromatics in environmental water purification. J. Colloid Interface Sci. 534, 357–369.
Que, Y., Feng, C., Zhang, S., Huang, X., 2015. Stability and catalytic activity of PEG-b-PS-capped gold nanoparticles: a matter of PS chain length. J. Phys. Chem. C 119, 1960–1970.
Sahoo, A., Tripathy, S.K., Dehury, N., Patra, S., 2015. A porous trimetallic Au@Pd@Ru nanoparticle system: synthesis, characterisation and efficient dye degradation and removal. J. Mater. Chem. A 3, 19376–19383.
Scurrell, M.S., 2017. Thoughts on the use of gold-based catalysts in environmental protection catalysis. Gold Bull. 50, 1–8.
Soğukömeroğulları, H.G., Karataş, Y., Celebi, M., Gülcan, M., Sönmez, M., Zahmakiran, M., 2019. Palladium nanoparticles decorated on amine functionalized graphene nanosheets as excellent nanocatalyst for the hydrogenation of nitrophenols to aminophenol counterparts. J. Hazard. Mater. 369, 96–107.
Song, P., He, L.-L., Wang, A.-J., Mei, L.-P., Zhong, S.-X., Chen, J.-R., Feng, J.-J., 2015. Surfactant-free synthesis of reduced graphene oxide supported porous PtAu alloyed nanoflowers with improved catalytic activity. J. Mater. Chem. A 3, 5321–5327.
Song, M., Wu, Y., Xu, C., Wang, X., Su, Y., 2019. Synergistic effects of multi-active sites in silver modified Bi^{0}-$BiVO_4$ toward efficient reduction of aromatic nitrobenzene. J. Hazard. Mater. 368, 530–540.
Wang, W., Xu, P., Chen, M., Zeng, G., Zhang, C., Zhou, C., Yang, Y., Huang, D., Lai, C., Cheng, M., Hu, L., Xiong, W., Guo, H., Zhou, M., 2018. Alkali metal-assisted synthesis of graphite carbon nitride with tunable band-gap for enhanced visible-light-driven photocatalytic performance. ACS Sustain. Chem. Eng. 6, 15503–15516.
Xia, J., He, G., Zhang, L., Sun, X., Wang, X., 2016. Hydrogenation of nitrophenols catalyzed by carbon black-supported nickel nanoparticles under mild conditions. Appl. Catal. B: Environ. 180, 408–415.
Xia, J., Zhang, L., Fu, Y., He, G., Sun, X., Wang, X., 2018. Nitrogen-doped carbon black supported $NiCo_2S_4$ catalyst for hydrogenation of nitrophenols under mild conditions. J. Mater. Sci. 53, 4467–4481.
Xiao, Q., Sarina, S., Waclawik, E.R., Jia, J., Chang, J., Riches, J.D., Wu, H., Zheng, Z., Zhu, H., 2016. Alloying gold with copper makes for a highly selective visible-light photocatalyst for the reduction of nitroaromatics to anilines. ACS Catal. 6, 1744–1753.
Xiong, W., Zeng, Z., Zeng, G., Yang, Z., Xiao, R., Li, X., Cao, J., Zhou, C., Chen, H., Jia, M., Yang, Y., Wang, W., Tang, X., 2019. Metal-organic frameworks derived magnetic carbon-αFe/Fe_3C composites as a highly effective adsorbent for tetracycline removal from aqueous solution. Chem. Eng. J. 374, 91–99.
Xu, P., Zeng, G.M., Huang, D.L., Feng, C.L., Hu, S., Zhao, M.H., Lai, C., Wei, Z., Huang, C., Xie, G.X., 2012. Use of iron oxide nanomaterials in wastewater treatment: a review. Sci. Total Environ. 424, 1–10.
Xue, W., Huang, D., Zeng, G., Wan, J., Zhang, C., Xu, R., Cheng, M., Deng, R., 2018. Nanoscale zero-valent iron coated with rhamnolipid as an effective stabilizer for immobilization of Cd and Pb in river sediments. J. Hazard. Mater. 341, 381–389.
Yang, Y., Zeng, Z., Zhang, C., Huang, D., Zeng, G., Xiao, R., Lai, C., Zhou, C., Guo, H., Xue, W., 2018. Construction of iodine vacancy-rich BiOI/Ag@ AgI Z-scheme heterojunction photocatalysts for visible-light-driven tetracycline degradation: transformation pathways and mechanism insight. Chem. Eng. J. 349, 808–821.
Yi, H., Yan, M., Huang, D., Zeng, G., Lai, C., Li, M., Huo, X., Qin, L., Liu, S., Liu, X., Li, B., Wang, H., Shen, M., Fu, Y., Guo, X., 2019. Synergistic effect of artificial enzyme and 2D nano-structured Bi2WO6 for eco-friendly and efficient biomimetic photocatalysis. Appl. Catal. B: Environ. 250, 52–62.
You, J.-G., Shanmugam, C., Liu, Y.-W., Yu, C.-J., Tseng, W.-L., 2017. Boosting catalytic

activity of metal nanoparticles for 4-nitrophenol reduction: modification of metal naoparticles with poly(diallyldimethylammonium chloride). J. Hazard. Mater. 324, 420–427.
Zeng, Y., Xu, H., Do, D.D., Nicholson, D., 2018. Adsorption of argon on graphitized carbon black preloaded with methanol, ammonia and water: the role of adsorption regions and adsorbates. Chem. Eng. J. 334, 1316–1327.
Zhang, C., Wang, W., Duan, A., Zeng, G., Huang, D., Lai, C., Tan, X., Cheng, M., Wang, R., Zhou, C., Xiong, W., Yang, Y., 2019. Adsorption behavior of engineered carbons and carbon nanomaterials for metal endocrine disruptors: experiments and theoretical calculation. Chemosphere 222, 184–194.
Zhao, X., Zhu, J., Liang, L., Li, C., Liu, C., Liao, J., Wei, X., 2014. Biomass-derived N-doped carbon and its application in electrocatalysis. Appl. Catal. B: Environ. 154–155, 177–182.
Zhao, J., Wang, B., Yue, Y., Di, S., Zhai, Y., He, H., Sheng, G., Lai, H., Zhu, Y., Guo, L., Li, X., 2018. Towards a greener approach for the preparation of highly active gold/carbon catalyst for the hydrochlorination of ethyne. J. Catal. 365, 153–162.
Zhou, X., Lai, C., Huang, D., Zeng, G., Chen, L., Qin, L., Xu, P., Cheng, M., Huang, C., Zhang, C., Zhou, C., 2018. Preparation of water-compatible molecularly imprinted thiol-functionalized activated titanium dioxide: selective adsorption and efficient photodegradation of 2, 4-dinitrophenol in aqueous solution. J. Hazard. Mater. 346, 113–123.
Zhou, C., Xu, P., Lai, C., Zhang, C., Zeng, G., Huang, D., Cheng, M., Hu, L., Xiong, W., Wen, X., Qin, L., Yuan, J., Wang, W., 2019. Rational design of graphic carbon nitride copolymers by molecular doping for visible-light-driven degradation of aqueous sulfamethazine and hydrogen evolution. Chem. Eng. J. 359, 186–196.